

# A search for Magnetic Clouds Associated with Coronal Mass Ejections

C. Cid, M. A. Hidalgo, J. Rodríguez-Pacheco, J. Medina, and J. Sequeiros  
*Departamento de Física, Universidad de Alcalá, Alcalá de Henares, Madrid, Spain*

## Abstract

It is generally believed that coronal mass ejections (CMEs) are the direct cause of about 1/3 of magnetic clouds (MCs). In sight of the new models for the magnetic geometry of the CMEs, the number of MCs related with CMEs is expected to be greater than that value. We have developed a model for the magnetic topology of MCs. Using that topology as the signature of MCs, we have attempted to identify the MCs from several spacecraft data related with CMEs from SMM. The results obtained indicate that every CME can be associated with a MC in the solar wind in a period from about 3 days to 5 days after its ejection from the Sun.

## 1 Introduction:

Burlaga et al. (1981) introduced the term magnetic cloud (MC) for a structure in the solar wind that followed an interplanetary shock and showed a smooth rotation of the magnetic field. Other features of these events are low temperatures and a high magnetic field strength.

Nowadays, the analysis of spacecraft data reveals that these events are common in the solar wind. About 1/3 of CMEs observed in the solar wind exhibit internal field rotations, characteristic of magnetic flux ropes. However, the relationship between the CMEs observed near the Sun and MCs is poorly understood.

These events are not always associated with interplanetary shocks but only when they travel faster than the ambient solar wind. Besides the identification of MCs locating cloud boundaries is an open problem [Lepping et al., 1990]. Zhang and Burlaga (1988) showed that the clouds are usually spatially shorter than the interval defined by counter-streaming electrons, suggesting that the clouds are parts of larger transient structures.

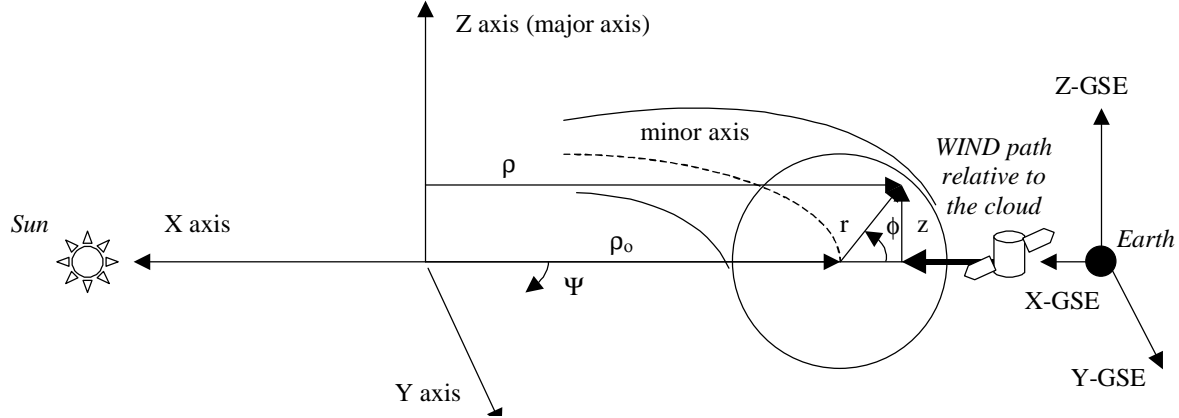
Recent studies have identified the boundary of MCs in terms of changes in thermodynamic properties of the plasma. This study has shown a deviation of the thermodynamic behavior of protons in the region near the boundaries of magnetic clouds compared with those that surround the cloud itself. There have been attempts to identify the MCs with one of the structures that CMEs show close to the Sun: the eruptive prominence or the cavity. At the present it is unclear how the flux rope topology associated with the MC arises, but there is evidence that MCs are magnetic flux ropes with helical field lines increasingly twisted at greater distances from the axis of the rope.

We present a simple model to identify MCs in the solar wind using the magnetic field vector from satellite observations. The model describes the magnetic structure of the cloud using a toroidal reference system and without assuming force-free condition.

## 2 Topology of Magnetic Clouds:

It is assumed that a MC may be represented as a flux rope. Thus, it seems convenient to describe it with a toroidal reference system.

There are two possible reference systems to describe every point in the torus. The first one, uses the major radius of the cloud,  $\rho$ , the toroidal coordinate,  $\psi$ , and the  $z$  Cartesian coordinate (see next figure). Instead of these coordinates, once we have the radius of the minor axis of the torus,  $\rho_0$ , we can use the minor radius,  $r$ , the toroidal coordinate,  $\psi$ , and the poloidal coordinate,  $\phi$ .



For the sake of simplicity, we consider the cloud as a loop that locally (as a first approximation) is a section of a circular torus with major central radius  $\rho_0$ .

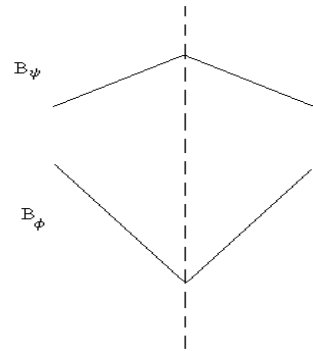
The spacecraft measures the magnetic field vector  $(B_x, B_y, B_z)$  in GSE-coordinates. However, in order to compare with our model, we transformed the measured magnetic field vector into a toroidal reference system (i.e., with a poloidal component,  $B_\phi$ , and a toroidal one,  $B_\psi$  for the flux tube topology that we assume for the MC). The  $B_r$  component is assumed to be zero. Thus, in our case we relate both finite toroidal coordinates with the GSE system through the expressions:  $B_\phi = \sqrt{B_x^2 + B_z^2}$ ,  $B_\psi = B_y$ .

## 3 The Model:

Describing the MCs with the topology explained in the previous section, we model them analyzing independently the toroidal and poloidal components of the magnetic field. The model determines the MC structure relating them to the corresponding poloidal and toroidal components of their current densities. We have also considered an ambient magnetic field decomposed in two contributions: a toroidal,  $B_\psi^{amb}$ , and a poloidal,  $B_\phi^{amb}$ . In these two components of the ambient field is included how far away is the spacecraft path from the axis of the magnetic cloud and the contribution of the tilt of the axis. The poloidal component of the magnetic field can be modeled by the effect of a finite current line generated by a current density in the toroidal direction. Assuming that the flux rope cross section has a circular shape, then the poloidal component inside the cloud can be written as [Cid et al.]:

$$B_\phi = B_\phi^{amb} + \frac{\mu_0}{2} j_\psi r$$

where  $\mu_0$  is the vacuum permeability,  $r$  is the minor radius of the cloud and  $j_\psi$  is the toroidal current density. Using this expression,



we assume that the current distribution is uniform in the cross section of the cloud. Thus, the poloidal component shows a minimum at the center of the cloud increasing linearly from this point (see the figure above).

Similarly, we assume that the toroidal magnetic field is due to the poloidal current  $j_\phi$ . Then, it is given by the expressions [Cid et al.]:

$$B_\psi = B_\psi^{amb} + \frac{\mu_0}{2} j_\phi \frac{(\rho_0 - r)^2 - (\rho_0 - R)^2}{(\rho_0 - r)}, \quad \rho < \rho_0$$

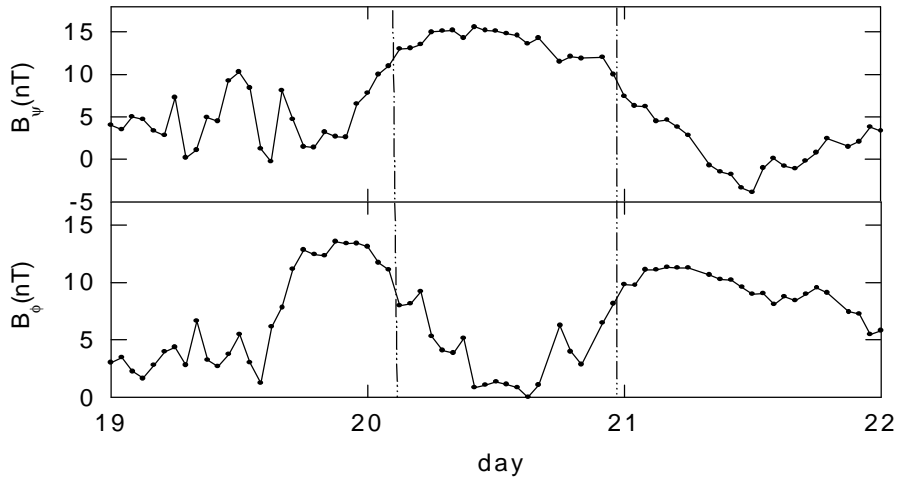
$$B_\psi = B_\psi^{amb} + \frac{\mu_0}{2} j_\phi \frac{(\rho_0 + r)^2 - (\rho_0 - R)^2}{(\rho_0 + r)}, \quad \rho > \rho_0$$

where  $R$  is the maximum cloud minor radius. Thus, the toroidal component of the magnetic field shows a maximum at the center decreasing toward the boundaries. See the figure above.

#### 4 Identification of Magnetic Clouds from CMEs:

The first step in order to identify MCs with the model is to transform the experimental magnetic field data (in GSE reference system) into the toroidal reference system (Section 2). The experimental data obtained from the spacecraft are expressed as a function of time. When the cloud passes through the spacecraft, the data at different time means data at different positions of the spacecraft related to the cloud axis. Thus, assuming a mean velocity for the cloud, it is expected to observe in the time profile the trend described in the figure of section 3. Hence, the criterion to identify MCs is based upon seeking the tendency shown in the figure over the experimental data, that must be satisfy simultaneously in both components of the magnetic field: the poloidal and toroidal component. We set the boundaries of the cloud where this behavior ends. We have found that in all clouds analyzed these boundaries coincide with a pronounced minimum in the experimental toroidal component of the magnetic field and simultaneously, a sharp maximum in the experimental poloidal component.

In next figure we show both components of the magnetic field, the poloidal and the toroidal, of a well-known cloud of 1980. The interval between both dashed vertical lines represent the cloud as it is determined by our model



In the next Table are detailed the clouds measured from several spacecraft data related with CMEs from SMM identify with the model presented. The results indicate that almost every CME can be associated with a MC in the solar wind in a period from about 3 days to 5 days after its ejection from the Sun.

Table: MCs identified with the model and related with CMEs from SMM during 1980

CME(mm-dd)	PA	MC(mm-dd-hh)	<v> (km/s)	$\Delta t$ (Days)
Mar 15/16	120	Mar 20 02	325	5.3
Mar 26	212	Mar 30 15	320	5.4
Mar 27	204			
GAP		Apr 05 23	510	3.4
Apr 07	320	Apr 11 06	500	3.5
Apr 14	005	Apr 19 13	320	5.4
Apr 14/15	313			
Apr 19	225	Apr 23 18	305	5.7
Apr 21-22	046			
Apr 30	066	May 05 10	335	5.2
May 1	240			
May 05	299	May 09 10	415	4.2
May 06	280	May 10 13	385	4.5
GAP		May 25 04	400	4.3
Jun 19/20	207	Jun 23 00	355	4.9
Jun 21/22	103	Jun 25 00	345	5.0
GAP		Jun 27 23	340	5.1
Jun 29	240	Jul 02 22	290	6.0
Jul 06	263	Jul 09 07	400	4.3
Jul 09	292	Jul 12 19	360	4.8
?		Jul 26 00	430	
Ago 10	287	Aug 13 06	320	5.4
Ago 11	052			
Ago 13	134	Aug 17 01	340	5.1
Ago 16/17	058	Aug 19 16	435	4.0
Ago 18	116	Aug 21 00	390	4.4
GAP		Ago 21 14	420	4.1
GAP		Ago 24 17	305	5.7
Ago 30/31	145	Sep 03 15	330	5.2
Sep 01	297			

**Acknowledgements.** This work has been supported by the Comision Internacional de Ciencia y Tecnología (CICYT) of Spain. Grant ESP97-1776.

### References

- Burlaga, L. F. et al., 1981, J. Geophys. Res. 86, 6673-6684  
 Burlaga, L. et al., 1998, J. Geophys. Res. 103, 277-285  
 Cid et al., 1998, 16<sup>th</sup> European Cosmic Ray Symposium, Editor J. Medina, 189-198  
 Lepping, et al., 1990, J. Geophys. Res. 95, 11957-11965  
 Zhang, G., and L. F. Burlaga, 1988, J. Geophys. Res. 93, 2511-2518